Effect of realistic focal conditions on the strong-field ionization of helium

J. P. Paquette and J. L. Chaloupka
Department of Physics, College of William and Mary, Williamsburg, VA 23187–8795, USA
(Received 26 January 2009; published 13 April 2009)

The results from classical three-dimensional simulations of the double ionization of helium in an intense laser field are presented for realistic nonparaxial focal conditions. The existence of an out-of-phase electric field component in the laser propagation direction produces an effective longitudinal ellipticity, resulting in a reduction in the double-ion yields as a function of position in the laser focus. It is found that under conditions of tight focusing, the effective focal volume for nonsequential double ionization is significantly reduced.

DOI: 10.1103/PhysRevA.79.043410 PACS number(s): 32.80.Rm, 32.80.Wr, 42.25.Ja

I. INTRODUCTION

In 1905, Einstein's description of the photoelectric effect changed our fundamental understanding of the interaction of light with matter. Since atoms appeared to only absorb a single quantum of light energy, low-frequency light could never lead to photoionization regardless of intensity [1]. In the 1960s, soon after the invention of the laser, it was shown that at sufficiently high intensities, the simultaneous absorption of multiple photons could lead to the ionization of atoms with large binding energies, even with weak infrared light [2]. Since then, theoretical treatments have often disposed of the quantum picture of light altogether, instead treating the intense laser field as completely classical and allowing for a quantum-mechanical atomic response. In this semiclassical picture, the Coulomb potential is so severely distorted by the laser field that an electron may tunnel through the suppressed barrier and become liberated. Double ionization may then result in a sequential fashion, from two effectively independent tunneling events, or in a direct manner, through a mechanism known as rescattering. In rescattering, a single electron is freed through tunnel ionization, propagates in the combined laser-Coulomb potentials, and is driven back by the laser field to the ion core leading to impact ionization [3]. Through this process, double ionization is observed to occur with much greater probability, and at much lower intensities, than is predicted through sequential tunnel ionization alone [4]. This is arguably the most fundamental phenomenon in strong-field laser physics, and its understanding plays an important role in the study of high-harmonic generation [5], attosecond pulse generation [6], and many other aspects of intense laser-matter interaction.

In 2001, Eberly and co-workers [7] pioneered a completely classical theoretical treatment that improved our physical insight into nonsequential double ionization (NSDI). Surprisingly, neglecting all quantum behavior did not diminish the qualitative agreement between their simulations and the experimental results of others. This emphasized the importance of the classical electron trajectories in determining the overall behavior of the ionization of atoms by intense laser fields. We now extend this approach to include a more realistic description of the physical properties of the laser focus, and in doing so, present a systematic study of the effects of describing the laser field beyond the paraxial approximation. In particular, the requirement that the divergence of the electric field must vanish leads to a nonzero field component along the propagation direction of the laser. The greatest impact from this longitudinal electric field comes from an out-of-phase term which results in a nontransverse "elliptical polarization" (in the plane of the laser polarization and the propagation directions). This can dramatically influence classical electron trajectories, strongly affecting rescattering, and under the right conditions, significantly impacting double-ionization yields. We present results from our three-dimensional fully classical simulations that show how the longitudinal field can be ignored in some cases and under what conditions its effects must be included.

II. OVERVIEW OF THE CLASSICAL SIMULATIONS

The two main components of our numerical simulation are the laser field, with realistic spatial and temporal variations, and the model atom. We employ the classical two-electron "atom" developed by Haan *et al.* [8] which approximates the behavior of a helium atom with purely classical interactions. The laser field is given by our extended paraxial treatment of a Gaussian focus (see Sec. III for a complete discussion) with a wavelength of 800 nm and a beam waist of 1, 5, or 10 μm. The pulse has a Gaussian intensity envelope with a full width at half maximum of 10 fs. The simulation begins at 26 fs before the peak of the pulse (corresponding to 9.75 optical cycles and a null in the electric field) where the electric field envelope is at 10^{-4} of its peak value. This gives the model atom time to stabilize while the laser is effectively "off" and also ensures that the turn on of the laser pulse is smooth. The initial position and momentum for each electron are chosen randomly for each run, with the requirement that the bound-state energy is correct for helium. Figure 1 shows the temporal evolution of the pulse, with a 1000× magnified view (along the vertical axis) of the start of the simulation. In this section we present a series of results demonstrating the accepted "standard" qualitative behavior of strong-field ionization in a laser field. These simulations take place at the center of the focal region with a beam waist of 5 μm. Here, the effects of the longitudinal electric field are negligible.

In order to help visualize and distinguish between sequential and direct double-ionization events, we first present individual events in the form of electron-nucleus distances as a function of time. Here, the peak intensity is set to

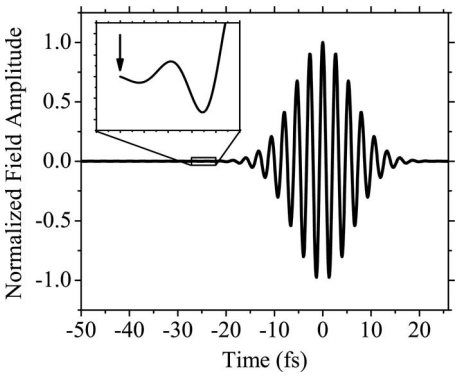

FIG. 1. The evolution of the normalized electric field amplitude for our Gaussian laser pulse is shown as a function of time. The inset shows the time at which the simulation begins, magnified along the vertical axis by a factor of 1000. The simulation starts at a null in the optical cycle where the electric field envelope is equal to 10^{-4} of its peak value.

2×10^{16} W/cm^2, where both sequential and direct double-ionization events are expected to take place. Figure 2 shows a sequential stepwise double-ionization event. The distance from the nucleus (on a logarithmic scale) for each electron is plotted as a function of time. Three distance ranges are shown on the figure, corresponding to a bound region ($<10^{-10}$ m), a region of strong *e-e* interaction (10^{-10}–10^{-9} m), and a free unbound region ($>10^{-9}$ m). In this example, one electron is liberated early in the evolution of the laser pulse and its trajectory takes it away from the ion core. As the laser intensity grows, the second electron is freed through an effectively independent second process. In Fig. 3, the peak intensity is decreased to 6×10^{15} W/cm^2, an intensity which leads to a higher proportion of nonsequential (direct) rescattering events. In this example, the trajectory of the first electron interacts strongly with the remaining bound electron, helping to liberate it from the nucleus. Here, both electrons are freed together in a single strongly *e-e* correlated event.

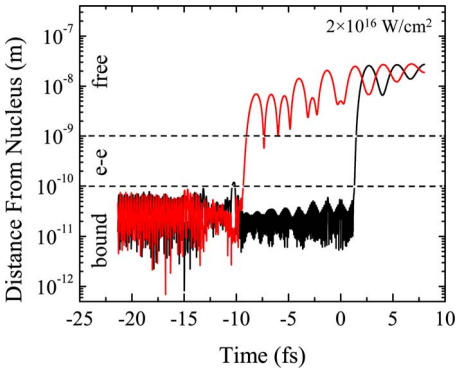

FIG. 2. (Color online) To help visualize a double-ionization event, the distance from the nucleus for each electron in the model atom is plotted as a function of time. Here, one electron (red line) is liberated early in the pulse and does not interact strongly with the ion core, and the second electron (black line) is liberated later in a similar independent fashion. This is an example of a sequential double-ionization event. The laser peak intensity is 2×10^{16} W/cm^2.

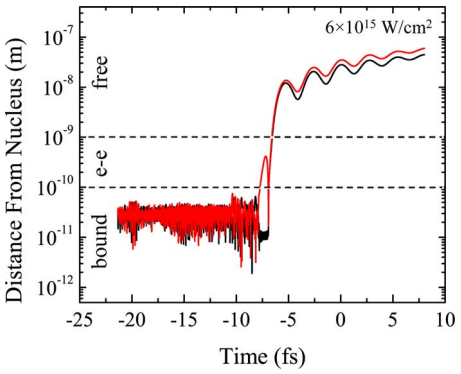

FIG. 3. (Color online) In this example of a nonsequential (direct) rescattering event, one electron (red line) is liberated by the field but is driven back strongly to the ion core, helping to free the second electron (black line). The laser peak intensity is 6×10^{15} W/cm^2.

The first experimental evidence of a direct path toward double ionization came in the form of yield curves that showed evidence of two different rates in the double-ion curves [4]. In the plots of ion yield versus peak laser intensity, a significant enhancement was observed in the double-ion yield over what was expected from a purely sequential picture. In the results from our simulations, the single and double-ionization "yields" are expressed as probabilities for ionization for a given peak intensity. This probability is equal to the ratio of single- or double-ionization counts to simulation runs. For each intensity, a large set of Monte Carlo simulations are performed in which the initial position and momentum for each electron are randomized at the beginning of each run, with the constraint that the total energy is correct for our model helium atom, and the total angular momentum is zero [8]. All other variables, such as peak intensity and the location of the atom within the laser focus, are held constant for a set of runs. In Fig. 4(a) we show the results from our simulations for a linearly polarized driving field. The single-ionization curve (red dashed line) exhibits a single rate leading to saturation, while the double-ionization curve (black solid line) shows two rates before saturating. Error bars here, and throughout this paper, are statistical and represent a single standard deviation along each direction, as determined by the point estimation of a proportion method [9]. The region of double-ionization enhancement, or the "knee," is shown shaded. Since we do not integrate over the focal volume, the curves we present differ from the experimental yield curves most notably at high intensities where our curves saturate. Typical experimental yields continue to rise past saturation due to the growth in the effective focal volume. The qualitative agreement, however, is unmistakable. The rates from a circularly polarized driving field are shown in Fig. 4(b). To enable a direct comparison with the results from a linearly polarized driving field, the intensity here and throughout this paper is scaled to the peak of the electric field amplitude, rather than to the cycle-averaged energy. For circular polarization, this shifts the intensity by a factor of 2, while for an ellipticity of 0.10, the intensity shift is equal to a factor of 1.01. Since an electron liberated by a circularly polarized field is never driven back to the ion core,

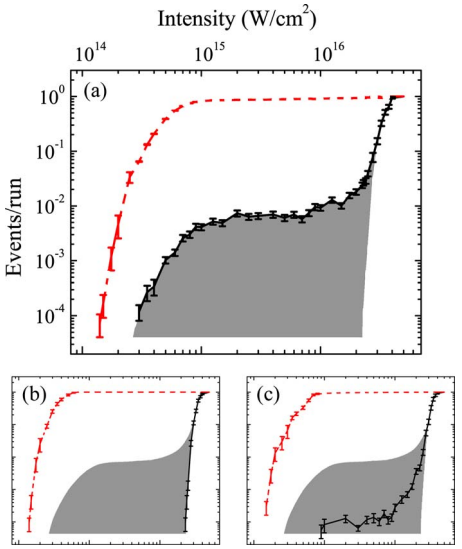

FIG. 4. (Color online) The rates, expressed as events per simulation run, for single (red dashed lines) and double (black solid lines) ionization as a function of laser intensity for (a) linearly ($\varepsilon=0.0$), (b) circularly ($\varepsilon=1.0$), and (c) elliptically ($\varepsilon=0.1$) polarized driving fields. The shaded region shows the double-ionization enhancement over the sequential rate for the linearly polarized case.

the region of double-ion enhancement is completely absent: rescattering is effectively turned off. An elliptically polarized driving field gives similar results, showing the importance of classical trajectories that are "on target" for recollision. Figure 4(c) shows the rates for an ellipticity of 0.10, defined as the ratio of the minor to major axis of the ellipse traced out by the electric field vector. The vertical and horizontal axes for Figs. 4(b) and 4(c) are identical to those in Fig. 4(a). Clearly, even a slight ellipticity greatly diminishes the likelihood for rescattering, in agreement with experiment [10].

More sophisticated experimental schemes have recently been employed to acquire correlated energy and momentum spectra [11,12]. In Fig. 5 we show the electron energy spectrum from our simulations correlated with single-(red circles) and double-(black squares) ionization events at an intensity

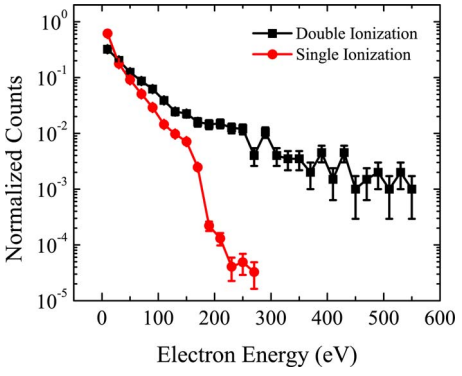

FIG. 5. (Color online) The energy spectra correlated with single (red circles) and double (black squares) ionization are plotted for an intensity of 6×10^{15} W/cm^2. The smooth extension to high energies for the double-ion case is in qualitative agreement with experiments.

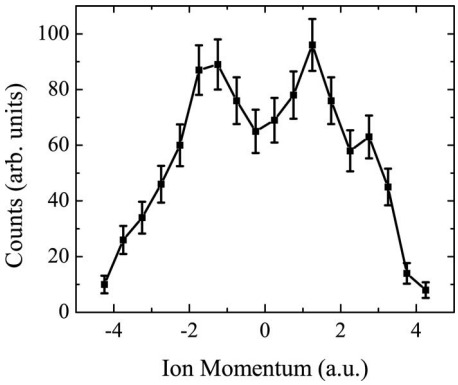

FIG. 6. The recoil ion momentum (along the polarization direction) correlated with double-ionization events is plotted for an intensity of 6×10^{14} W/cm^2. The double-peaked structure is expected from rescattering and is in qualitative agreement with experiments.

of 6×10^{15} W/cm^2. Our results are in qualitative agreement with experimental work [11], where the electrons correlated with the double ionization of helium are "warmer," corresponding to a distribution that extends smoothly to high energies. In Fig. 6, the ion momentum distribution (along the polarization direction) is plotted for double-ionization events at a peak intensity of 6×10^{14} W/cm^2. The double-peaked ion momentum is expected from the rescattering model and is consistent with experimental observations [12]. These results also agree with previous classical three-dimensional simulations performed by Haan *et al.* [13] and give further confirmation that the fully classical approach nicely reproduces familiar experimental behavior.

The results presented in this section have shown that the basic ionization behavior observed in experiments is qualitatively reproduced here, as long we probe regions in the laser focus where the longitudinal electric field can be neglected. In Sec. III, we show where in the laser focus these effects become appreciable and in Sec. IV demonstrate how the double-ionization yields change as a consequence.

III. LONGITUDINAL ELECTRIC FIELD AND EFFECTIVE ELLIPTICITY

We model strong-field ionization using a more complete description of a Gaussian laser field than is typically considered. In the simplest description, the magnitude of the electric field is given by the paraxial approximation and its direction is taken to be perpendicular to the laser propagation direction [14]. This has been shown to be incomplete as it violates Maxwell's requirement that the divergence of the field be zero [15]. Naturally, this violation becomes more severe as the focusing is tightened and the spatial gradients increase.

Lax *et al.* [15] derive a correction term which serves to satisfy Maxwell's equations more completely. Davis [16] expands on that work by developing an approach that leads to even higher accuracy. One feature of Davis' approach is that the equations can be written in dimensionless variables

$$\xi = \frac{x}{w_0}, \quad \eta = \frac{y}{w_0}, \quad \zeta = \frac{z}{z_0}, \tag{1}$$

where w_0 is the beam waist and z_0 is the Rayleigh range. Since we will be dealing with linear polarization, x is the distance along the polarization direction, y is the distance along the other transverse direction, and z is the distance along the laser propagation direction. In the dimensionless form of the field equations, we can define

$$s = \frac{w_0}{z_0} = \frac{2}{kw_0}, \tag{2}$$

where $k = \frac{2\pi}{\lambda}$ and s is the ratio of the focal region's transverse and longitudinal extents. If the beam waist is large compared to the wavelength, s will be less than 1, making it a suitable expansion parameter (this expansion is valid even for our examples of tight focusing, namely, $\lambda = 800$ nm and $w_0 = 1$ μm, giving $s = 0.25$). The other key feature is that, unlike Lax *et al.* who restrict the electric field to be linearly polarized, Davis only requires that the vector potential be linearly polarized, which simplifies the derivation. The vector potential is then given by

$$\mathbf{A}(\mathbf{r}) = \psi(\mathbf{r}) e^{-ikz} \hat{x} \tag{3}$$

and the expansion takes the form

$$\psi = \psi_0 + s^2 \psi_2 + s^4 \psi_4 + \cdots . \tag{4}$$

The components of ψ can be found by solving the wave equation for the vector potential in free space. The electric and magnetic field components can be found by substituting the expressions for ψ and $\mathbf{A}(\mathbf{r})$ into

$$\mathbf{E} = \frac{i}{k} \nabla (\nabla \cdot \mathbf{A}) + ik\mathbf{A}, \tag{5}$$

$$\mathbf{B} = \nabla \times \mathbf{A}. \tag{6}$$

Terms are then grouped in orders of s. The zeroth-order terms yield only field components for E_x and B_y (and recovers the paraxial approximation). The first-order terms contribute to E_z and B_z and are equivalent to the results of Lax *et al.* An important aspect of these results is that E_z contains two terms: one in-phase with E_x and the other shifted by 90° with respect to E_x. This arises due to the fact that the propagation term is given by e^{-ikz}, so a factor of i will be extracted from the exponential when the operation $\nabla(\nabla \cdot \mathbf{A})$ is performed on A_z.

Corrections of even higher order in s can be obtained [17], with even powers of s contributing to the transverse components of the electric and magnetic fields, and odd powers contributing to the longitudinal components. For the laser parameters we will be working with, a description using terms through the third order will be used in all of our simulations when dealing with the "corrected" form of the laser focus. This leads to maximal deviations from Maxwell's equations that are well below 1%, as defined by Barton and Alexander [18].

For the study of strong-field ionization, the most significant addition to the paraxial approximation is the lowest-order term of E_z due to its impact on the classical trajectories of the liberated electrons. For a free electron in the presence of a laser field polarized in the x direction, the dynamics are described by the Lorentz force $\mathbf{F} = q(\mathbf{E} + v \times \mathbf{B})$. If the paraxial approximation is used, $\mathbf{E}(\mathbf{r}) = (E_X, 0, 0)$ and $\mathbf{B}(\mathbf{r}) = (0, B_y, 0)$, then the electron's motion in the propagation direction is governed only by the term $v_x B_y$. In Fig. 7(a) we show the trajectory of a free electron released at the peak of the field in a plane wave of intensity 1×10^{15} W/cm^2. The oval at the start of the path represents a circle with a 1 Å diameter, appearing distorted due to the unequal vertical and horizontal scales. At this intensity, the effect of $\mathbf{v} \times \mathbf{B}$ is small enough that the electron returns very near to its parent ion. If an in-phase E_z term is added, whose amplitude is 10% of that of E_x, the electron will travel along a tilted path that again brings it close to recollision [Fig. 7(b)]. However, if an out-of-phase E_z term is included, again with amplitude that is 10% of E_x, the resulting trajectories are dramatically different. Depending on the sign of E_z, the electron will be pushed far away from the starting location in either direction [Figs. 7(c) and 7(d)]. This is reminiscent of the trajectory that an electron takes when driven by an elliptically polarized field, but the path is in a longitudinal, rather than transverse, direction. The presence of an out-of-phase longitudinal component of the electric field gives rise to a phenomenon we will refer to as an *effective ellipticity*.

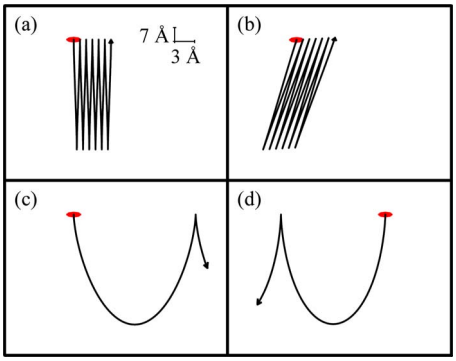

FIG. 7. (Color online) Simple free-electron trajectories demonstrate the importance of an out-of-phase component in the longitudinal electric field to rescattering. The red oval at the start of each path represents a circle with a 10 Å diameter, appearing distorted due to the unequal vertical and horizontal scales. In all, but the first case, the magnitude of the longitudinal component is equal to one tenth of the transverse term. (a) With E_z set to zero, the electron returns near to the "parent ion." (b) With an in-phase E_z, the slanted trajectory results from a tilted, but still linear, polarization, again resulting in close returns. An out-of-phase E_z drives the electron far from recollision due to the longitudinal "kick" it receives. Depending on the relative phase between the longitudinal and transverse components (+90° or −90°), this drift can be in the (c) $+z$ or (d) $-z$ direction.

For a plane wave, elliptical polarization refers to an electric field vector that is always perpendicular to the direction of propagation, but that has nonzero components along both transverse directions. As these terms are 90° out of phase, the electric field vector traces out an ellipse. Our description of the laser polarization is linear, but the addition of the out-of-phase E_z term skews this, resulting in "elliptical polariza-

tion," but in the xz plane. We will demonstrate that this effective ellipticity affects NSDI in much the same way that ordinary elliptical polarization does, but with varying strength throughout the laser focus.

The magnitude of the effective ellipticity depends on the laser focus parameters. The first-order correction results in an "ellipticity" of

$$\varepsilon_{\text{eff}} = \frac{E_x}{E_z} = \frac{2x}{kw_0^2[1 + (z/z_0)^2]^2}, \tag{7}$$

where E_x is the transverse field component, E_z is the out-of-phase longitudinal component, x and z are the distances along the polarization and propagation directions, respectively, k is the wave vector, and w_0 and z_0 are the beam waist and Rayleigh range, respectively. For simplicity, we do not include the effect of an in-phase component of E_z in Eq. (7) which slightly distorts the electric field ellipse away from $z=0$.

At large transverse distances, ε_{eff} can be quite large, but only for small beam waists will this occur in a region of high intensity. For example, in the focal plane ($z=0$), an effective ellipticity of 0.10 can be found at a normalized transverse distance of

$$\frac{x}{w_0} = \frac{kw_0}{20}. \tag{8}$$

For 800 nm laser light focused to a 10 μm beam waist, this gives a location $4w_0$ from the laser axis, where the peak intensity drops by a factor of 10^{14}. For a more tightly focused beam, such as a 1 μm beam waist, the location of interest reduces to $0.8w_0$, where the intensity is nearly one third the peak intensity at the center of the laser focus. The overall picture is shown in Fig. 8, where isoellipticity contours (shown in gray) are plotted together with the $1/e^2$ intensity contour (dashed) for three different beam waists. The region shaded black represents a region of $\varepsilon_{\text{eff}} \geq 0.10$. For a beam waist of 10 μm, shown in Fig. 8(a), the 0.10 isoellipticity contour is located far from the region of significant intensity. In Fig. 8(b), the beam waist is reduced to 5 μm, shifting the regions of sizeable effective ellipticity closer to the center of the laser focus. Finally, Fig. 8(c) depicts the situation with a 1 μm beam waist. Here, the 0.10 isoellipticity contour is found well within the $1/e^2$ intensity volume. Clearly, under tight focusing conditions, the effect of the effective ellipticity on rescattering should be carefully considered.

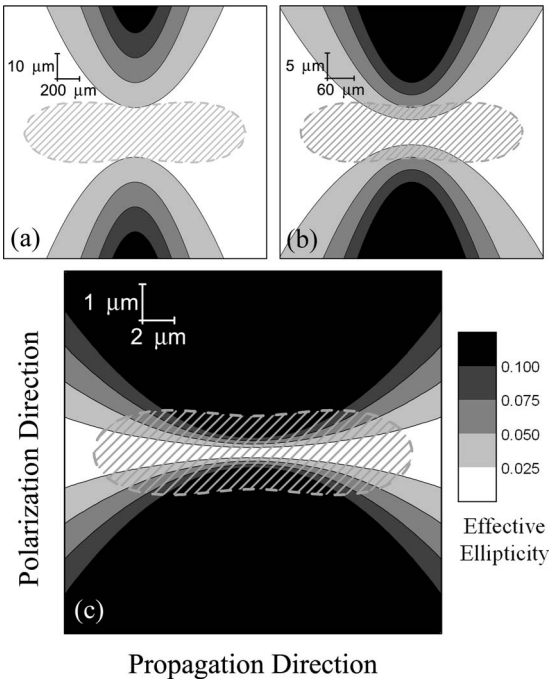

FIG. 8. The distribution of regions of varying effective ellipticity is plotted for three different beam waists. In each case, the volume bounded by the $1/e^2$ intensity is outlined with a dashed line. The ellipticity contours are shaded in gray, with the black region representing $\varepsilon_{\text{eff}} \geq 0.10$. In each case, the laser wavelength is set to 800 nm, and the beam waists are (a) $w_0=10$ μm, (b) $w_0=5$ μm, and (c) $w_0=1$ μm. For tight focusing conditions, regions of significant effective ellipticity exist within the focal volume.

IV. DOUBLE IONIZATION THROUGHOUT THE FOCAL VOLUME

In Sec. II, we have shown that our classical simulations (within the center of the focal region) qualitatively reproduce the expected ion yield curves, electron energy spectra, and ion recoil momenta in strong-field ionization. In Sec. III we showed that elsewhere within the focus there exist regions with a nonzero out-of-phase longitudinal component of the electric field, giving rise to a significant effective ellipticity. We now present the results of double-ionization yields taken throughout the laser focus. In order to make fair comparisons between the various locations, we first present results in which the intensity values are adjusted such that the local peak intensity is fixed for all locations. As a result, any variation in the observed yields is attributed to the local variance of the vector form of the laser field and not merely the spatial intensity envelope. Of course, this is an artificial condition placed on the simulations, but it serves to highlight the results that we will also study under realistic physical circumstances.

First, we show that the effective ellipticity affects NSDI yields in the same way as the ordinary transverse ellipticity does. As shown in Eq. (7), for given focusing conditions the effective ellipticity is dependent solely on the position within the laser focus. By holding the longitudinal position fixed at $z=0$ and using 800 nm wavelength and a 5 μm beam waist, the relationship between the transverse distance and effective ellipticity is given by $\varepsilon_{\text{eff}}=0.01$ $(x/\mu\text{m})$. Therefore, yields at different effective ellipticities can be determined by simply probing different positions along the polarization axis. In Fig. 9 we show the double-ion yields, in terms of the average number of ionization events per simulation run, at an intensity of 6×10^{15} W/cm^2 taken under conditions of transverse or effective ellipticity. The yields taken at the center of the laser focus for several different values of transverse ellipticity (red circles) overlap nicely with the yields from a linearly polarized beam, but at different locations along the polarization axis (black squares), and therefore at different effective ellipticities. Clearly, the presence of a nonzero effective el-

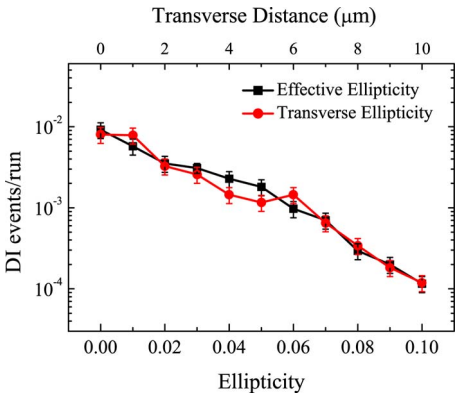

FIG. 9. (Color online) Double-ionization yields, expressed as events per simulation run, are significantly reduced under both ordinary (transverse) and effective (longitudinal) ellipticities. The yields taken with linear polarization, but at different transverse locations along $z=0$ (black squares), match well with yields due to equivalent changes to the driving field ellipticity (red circles) but at the center of the focal region. In all cases, the local peak intensity is held fixed at 6×10^{15} W/cm^2 and $w_0=5$ μm. This demonstrates that the effective ellipticity found within a linearly polarized laser focus has the same effect on reducing double-ion yields as a true elliptically polarized driving field.

lipticity reduces the NSDI count just as an ordinary elliptically polarized driving field would.

In Fig. 10 we show yield curves where the double-ionization knee is suppressed as a function of the distance from the center of the focus. For each of the three transverse positions, the local peak intensity is shown along the horizontal axis, and the yield is plotted along the vertical axis. The laser field is described utilizing the full correction described in Sec. III, most notably including the longitudinal electric field term E_z.

We now look at the double-ionization yields for a single intensity within the knee ($I=6\times10^{15}$ W/cm^2) as a function of the polarization direction x and along $z=0$ for three different spot sizes. This will help to determine the extent of the

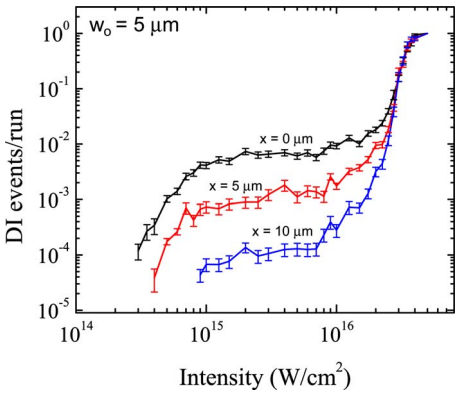

FIG. 10. (Color online) Double-ion yield curves taken for three transverse locations in a $w_0=5$ μm laser focus demonstrate the reduction (due to changes in the effective ellipticity) in the double-ionization enhancement (knee) as a function of position in the laser focus. The horizontal axis represents the local peak intensity for each position.

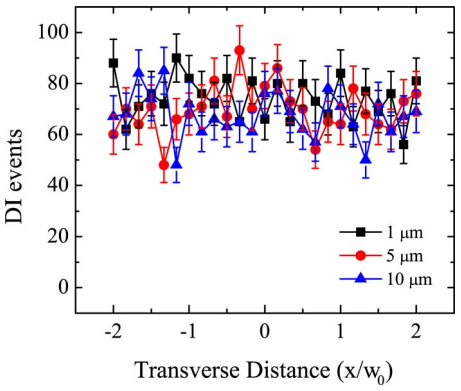

FIG. 11. (Color online) Double-ionization yields, expressed as events per 10 000 simulation runs, as a function of normalized transverse position are plotted for three different spot sizes with E_z set to zero. In all cases the local peak intensity is set to 6×10^{15} W/cm^2. Not surprisingly, the yields are unaffected by position or spot size.

NSDI suppression within a real laser focus. In Figs. 11–14, the horizontal axis shows the transverse position normalized to the laser spot size (x/w_0), and the vertical axis gives the number of double-ionization events per 10 000 simulation runs. In Figs. 11 and 12, the *local* peak intensity is held fixed, and in Figs. 13 and 14 the true peak intensity is held fixed. For each pair of figures, the paraxial description is used in the first figure (no E_z) and the full corrected form is used in the second figure (full E_z).

In the typical paraxial approach, and with the local peak intensity set fixed, we would expect the generated yield to be constant regardless of position and spot size. We check this by setting the E_z term to zero, and indeed, as shown in Fig. 11, the yields are constant. Turning E_z on, we find a sharp reduction as a function of x, as shown in Fig. 12. This is a result of the effective ellipticity created by the out-of-phase E_z term. As was shown in Fig. 8, the effective ellipticity is larger within the focal volume of a tightly focused beam. As

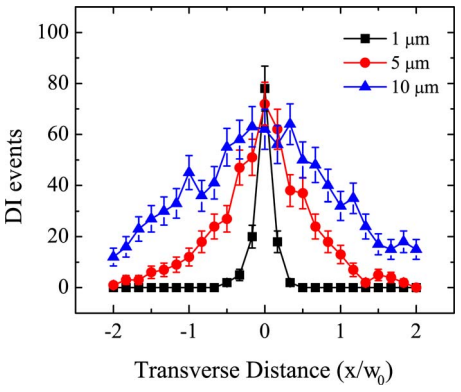

FIG. 12. (Color online) Double-ionization yields as a function of normalized transverse position are plotted for three different spot sizes using the complete description (beyond the paraxial approximation) of the fields in the laser focus. In all cases the local peak intensity is set to 6×10^{15} W/cm^2. The effect of E_z away from the center of the focus significantly reduces the double-ion yields, especially for the $w_0=1$ μm case.

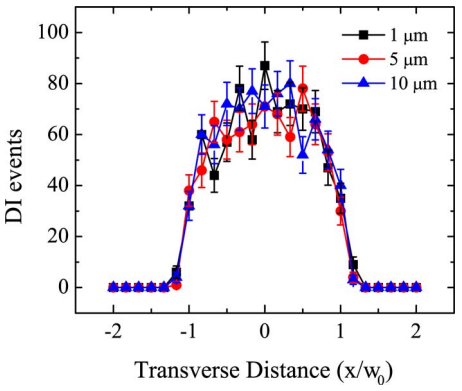

FIG. 13. (Color online) Double-ionization yields as a function of normalized transverse position are plotted for three different spot sizes with E_z set to zero. Here, the true peak intensity is set to 6×10^{15} W/cm^2. The dropoff in yield away from the center of the focus is due solely to a reduction in intensity and is the same regardless of spot size. The broad distribution is due to the flat intensity-insensitive region of the double-ion knee and results in a large effective focal volume.

a result, the double-ion yield falls off more quickly (relative to w_0) for small spot sizes.

Under realistic experimental conditions, the laser intensity falls off as a function of the distance from the center of the focus. The observed dropoff in double-ionization yield as a function of transverse position will be due to a combination of two factors: the falling laser intensity and the changing effective ellipticity. However, since we are probing intensities within the flat portion of the NSDI knee, the generation of double ions is actually quite insensitive to changes in intensity, so the effect of E_z should be more readily apparent. In Fig. 13 (E_z turned off) and Fig. 14 (E_z turned on) we show the yields as a function of transverse position for the three spot sizes but with the true peak intensity (at the center of the

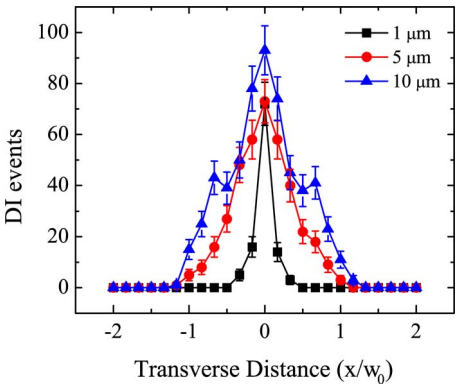

FIG. 14. (Color online) Double-ionization yields as a function of normalized transverse position are plotted for three different spot sizes using the complete description of the fields in the laser focus. Here, the true peak intensity is set to 6×10^{15} W/cm^2. The dropoff in yield away from the center of the focus is due to *both* a reduction in intensity and the effect of E_z. These plots represent realistic experimentally correct conditions and demonstrate the reduction in the effective focal volume for double ionization under tight focusing conditions.

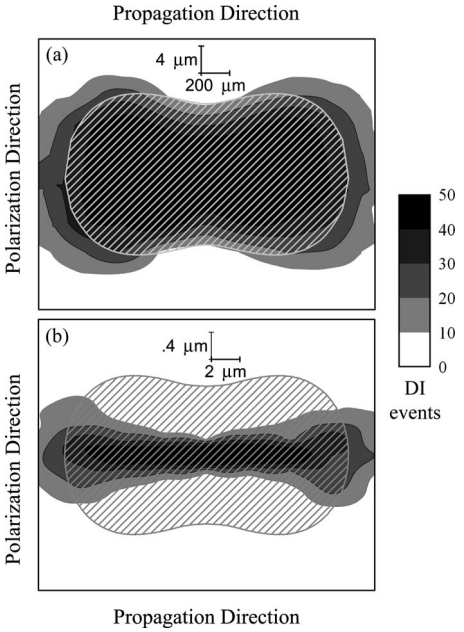

FIG. 15. The xz slices of double-ion yields at a peak intensity of 6×10^{15} W/cm^2 are shown for a beam waist of (a) $w_0 = 10$ μm and (b) $w_0 = 1$ μm. In both cases, the $1/e^2$ isointensity contour is depicted with a gray line, and the yields, expressed as double-ionization events per 10 000 simulations runs, are shown shaded. (a) For the loose focusing case, the region of significant double-ion yield fills the focal volume. (b) Under tighter focusing, the effective (scaled) focal volume is greatly reduced as a consequence of the longitudinal electric field.

laser focus) set to $I_{\text{peak}} = 6 \times 10^{15}$ W/cm^2. As shown in Fig. 4(a), the double-ion yield is relatively constant even as the intensity drops by a factor of 10 below I_{peak}. In Fig. 13, the double-ion yield as a function of normalized transverse distance is shown for three spot sizes within the paraxial description. Not surprisingly, all three cases give significant double-ion yields out to a full beam waist away from the center of the focus, resulting in a large effective focal volume. When the full correction is included, all of the yields are reduced due to the effects of the effective ellipticity. Of course, since reducing the spot size brings the regions of significant effective ellipticity closer to the center of the focal region, the effect is most severe for the tightest focusing ($w_0 = 1$ μm).

While we have shown here only the yields as a function of x for $z = 0$, the double-ion yields for any nonzero value of x will be reduced due to the effect of the longitudinal electric field. In Fig. 15 we show the double-ion yields throughout the xz plane at a peak intensity of 6×10^{15} W/cm^2 for loose and tight focusing conditions. The plots are scaled such that the $1/e^2$ isointensity contours (shown with a gray line) are the same size for each case. The double-ion yields, expressed as counts per 10 000 simulation runs, are shown shaded. For a beam waist of $w_0 = 10$ μm, the region of significant double-ion production fills the focal volume [Fig. 15(a)]. But for tight focusing ($w_0 = 1$ μm), the effective focal volume is dramatically reduced [Fig. 15(b)].

While constructing the complete volume-integrated yield curves is too computationally intensive for our current simu-

lations, it is clear that a reduction in the effective focal volume for NSDI relative to the full focal volume for sequential events would have a real effect on the shape of yield curves. In making direct precise comparisons between experimental results and theoretical predictions, these effects must be considered. The gap between theoretical and experimental works could be bridged in a number of ways. For example, a quantum-mechanical calculation which includes the full nonparaxial description of the laser field could be compared directly to experiment. Alternatively, experimenters could limit the effects of E_z by sampling a small region of the focal volume. By simply masking portions of the laser focus, volume effects have been shown to be reduced [19]. But in this case, regions of varying effective ellipticity still contribute to the total ion signal. Recently, a sophisticated ion spectrometer capable of resolving contributions from relatively small regions in the focal volume has been developed [20]. Unfortunately, the spatial resolution of such a device is ultimately limited by the thermal distribution of the target atoms in the backfilled chamber, and as a result a completely "clean" ion signal, from a region of well-defined peak intensity and effective ellipticity, is still not possible. In the end, as long as theoretical computations, complete with the longitudinal field effects, match the laboratory conditions, precise comparisons between numerical and experimental results should be possible.

V. FUTURE WORK

The effect of the longitudinal electric field (E_z) on classical electron trajectories, and in turn on the rescattering process, can be quite large. As a result, the observable double-ion yield can vary widely from different regions within the laser focus. A straightforward method to probe the effects of E_z would be to look at the typical volume-integrated ion yields, but for very tight focusing conditions. As we have shown, an 800 nm laser beam focused to a spot size of 1 μm generates significant longitudinal fields within regions of high intensity. The contribution to the total ion yield has been approximated in Sec. IV, and this effect could be readily mapped out in an experiment. Our simulations show very similar behavior in regions of effective (longitudinal) and true (transverse) ellipticity. Ion yield data taken for different focusing conditions would verify this connection.

An extension of this work, and perhaps the most interesting future direction for research, would be to study the effects of E_z at very high intensities. Here, the effect of $\mathbf{v}\times\mathbf{B}$ on electron trajectories is very large and always acts to push electrons away from the parent ion along the direction of laser propagation. Since E_z acts precisely along this direction, and has an out-of-phase component, it is a perfect candidate to counter the effects of $\mathbf{v}\times\mathbf{B}$ and to enhance the effects of rescattering at high intensities. Experimental and computational works have already shown that rescattering is an important component of ultrastrong-field ionization [21]. Simulations have also demonstrated the importance of the longitudinal electric field on affecting electron dynamics in ultraintense relativistic fields [22]. In Fig. 16 we show two sample free-electron trajectories for electrons in an intense

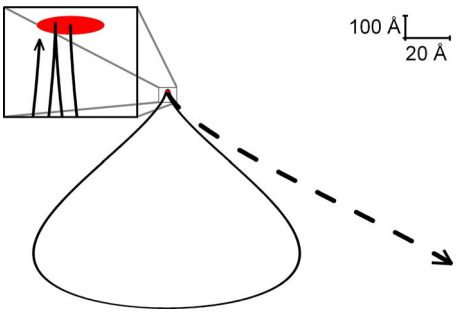

FIG. 16. (Color online) Free-electron trajectories for electrons released at the peak of an optical cycle in a 10^{18} W/cm^2 plane wave are shown for E_z=0 (dashed line) and a carefully chosen nonzero E_z (solid line). In the latter case, the effects of E_z and $\mathbf{v}\times\mathbf{B}$ cancel nearly perfectly, resulting in multiple returns to the parent ion (inset). The red oval represents a circle with a 10 Å diameter, appearing distorted due to the unequal vertical and horizontal scales.

plane wave. In both cases an electron was released at the peak of an optical cycle for an 800 nm laser at 10^{18} W/cm^2. The case of no E_z is shown as a dashed line. The longitudinal motion is due purely to the effect of $\mathbf{v}\times\mathbf{B}$, and the electron is clearly driven far from its parent ion. The solid line shows the trajectory with a nonzero E_z. Here, the effective ellipticity is chosen carefully (ε_{eff}=0.1748) such that the effects from $\mathbf{v}\times\mathbf{B}$ and E_z cancel nearly perfectly (appearing as a single closed loop), resulting in multiple returns to the parent ion (inset). Even though there exists a somewhat delicate balance between intensity and effective ellipticity, it is reasonable to expect that some regions within the focal volume will exhibit significant enhancement of double ionization. Simulations have already shown that high-harmonic generation at high intensities and with tight focusing are influenced by the longitudinal electric field [23]. We imagine that, in principle, the regions of enhanced and suppressed harmonic generation could even be controlled by shaping the input laser beam. By generating regions of intense spatial gradients, E_z could be modified selectively, generating regions of controlled enhanced harmonic generation. The effects of E_z at high intensities and within a modified laser focus are the subjects of our current and future studies.

VI. CONCLUSIONS

Classical three-dimensional simulations of a two-electron model atom interacting with an intense laser pulse have been performed. These computations are effective in qualitatively reproducing experimentally observed phenomena, including the knee structure of double-ionization yield curves generated with linearly polarized laser light and the suppression of the knee with increased ellipticity. We also observe a suppression of the double-ion yield for linearly polarized light, but in regions away from the center of the focal region. This phenomenon is a result of the presence of a longitudinal electric field, in particular a component that is 90° out of phase with the transverse electric field. This results in an effective elliptical polarization that is oriented in the longi-

tudinal plane. Under typical focusing conditions, this effect is minimized due to the local intensity decreasing at a faster rate than the increase in the effective ellipticity as a function of transverse displacement within the focal volume. However, under tight focusing conditions (e.g., $w_0=1$ μm for $\lambda=800$ nm laser light), the impact of the effective ellipticity is significant, resulting in a decrease in the effective focal volume for double-ion production. In making precise comparisons between theoretical and experimental results, the influence of the effective ellipticity should be considered.

ACKNOWLEDGMENTS

The work presented in this paper was made possible by support from the College of William & Mary and the Jeffress Memorial Trust.

[1] A. Einstein, Ann. Phys. **17**, 132 (1905); A. B. Arons and M. B. Peppard, Am. J. Phys. **33**, 367 (1965).

[2] G. S. Voronov and N. B. Delone, JETP Lett. **1**, 66 (1965); P. Agostini, F. Fabre, G. Mainfray, G. Petite, and N. K. Rahman, Phys. Rev. Lett. **42**, 1127 (1979).

[3] M. Yu Kuchiev, JETP Lett. **45**, 404 (1987); P. B. Corkum, Phys. Rev. Lett. **71**, 1994 (1993); K. J. Schafer, B. Yang, L. F. DiMauro, and K. C. Kulander, *ibid.* **70**, 1599 (1993).

[4] A. L'Huillier, L. A. Lompre, G. Mainfray, and C. Manus, Phys. Rev. A **27**, 2503 (1983); D. N. Fittinghoff, P. R. Bolton, B. Chang, and K. C. Kulander, Phys. Rev. Lett. **69**, 2642 (1992); B. Walker, B. Sheehy, L. F. DiMauro, P. Agostini, K. J. Schafer, and K. C. Kulander, *ibid.* **73**, 1227 (1994).

[5] A. McPherson, G. Gibson, H. Jara, U. Johann, T. S. Luk, I. A. McIntyre, K. Boyer, and C. K. Rhodes, J. Opt. Soc. Am. B **4**, 595 (1987); A. L'Huillier and Ph. Balcou, Phys. Rev. Lett. **70**, 774 (1993); C. Winterfeldt, C. Spielmann, and G. Gerber, Rev. Mod. Phys. **80**, 117 (2008).

[6] P. M. Paul, E. S. Toma, P. Breger, G. Mullot, F. Auge, Ph. Balcou, H. G. Muller, and P. Agostini, Science **292**, 1689 (2001); A. Scrinzi, M. Yu Ivanov, R. Kienberger, and D. M. Villeneuve, J. Phys. B **39**, R1 (2006).

[7] R. Panfili, J. H. Eberly, and S. L. Haan, Opt. Express **8**, 431 (2001).

[8] S. L. Haan, L. Breen, A. Karim, and J. H. Eberly, Phys. Rev. Lett. **97**, 103008 (2006).

[9] D. Schiff and R. B. D'Agostino, *Practical Engineering Statistics* (Wiley, New York, 1996), p. 106.

[10] P. H. Bucksbaum, M. Bashkansky, R. R. Freeman, T. J. McIlrath, and L. F. DiMauro, Phys. Rev. Lett. **56**, 2590 (1986); D. N. Fittinghoff, P. R. Bolton, B. Chang, and K. C. Kulander, Phys. Rev. A **49**, 2174 (1994); P. Dietrich, N. H. Burnett, M. Ivanov, and P. B. Corkum, *ibid.* **50**, R3585 (1994).

[11] R. Lafon, J. L. Chaloupka, B. Sheehy, P. M. Paul, P. Agostini, K. C. Kulander, and L. F. DiMauro, Phys. Rev. Lett. **86**, 2762 (2001).

[12] T. Weber, M. Weckenbrock, A. Staudte, L. Spielberger, O. Jagutzki, V. Mergel, F. Afaneh, G. Urbasch, M. Vollmer, H. Giessen, and R. Dörner, Phys. Rev. Lett. **84**, 443 (2000); R. Moshammer, B. Feuerstein, W. Schmitt, A. Dorn, C. D. Schröter, J. Ullrich, H. Rottke, C. Trump, M. Wittmann, G. Korn, K. Hoffmann, and W. Sandner, *ibid.* **84**, 447 (2000).

[13] S. L. Haan, J. S. Van Dyke, and Z. S. Smith, Phys. Rev. Lett. **101**, 113001 (2008).

[14] P. W. Milonni and J. H. Eberly, *Lasers* (Wiley, New York, 1988), pp. 484–490.

[15] M. Lax, W. H. Louisell, and W. B. McKnight, Phys. Rev. A **11**, 1365 (1975).

[16] L. W. Davis, Phys. Rev. A **19**, 1177 (1979).

[17] L. Cicchitelli, H. Hora, and R. Postle, Phys. Rev. A **41**, 3727 (1990).

[18] J. P. Barton and D. R. Alexander, J. Appl. Phys. **66**, 2800 (1989).

[19] P. Hansch, M. A. Walker, and L. D. Van Woerkom, Phys. Rev. A **54**, R2559 (1996).

[20] J. Strohaber and C. J. G. J. Uiterwaal, Phys. Rev. Lett. **100**, 023002 (2008).

[21] S. Palaniyappan, A. DiChiara, I. Ghebregziabher, E. L. Huskins, A. Falkowski, D. Pajerowski, and B. C. Walker, J. Phys. B **39**, S357 (2006).

[22] A. Maltsev and T. Ditmire, Phys. Rev. Lett. **90**, 053002 (2003); S. Masuda, M. Kando, H. Kotaki, and K. Nakajima, Phys. Plasmas **12**, 013102 (2005).

[23] Q. Lin, S. Li, and W. Becker, Opt. Lett. **31**, 2163 (2006).